Neutron multiplicity distributions for 1.94 to 5 GeV/*c* proton-, antiproton-, pion-, kaon-, and deuteron-induced spallation reactions on thin and thick targets

L. Pienkowski,* F. Goldenbaum, D. Hilscher,† and U. Jahnke
Hahn-Meitner-Institut Berlin, Glienickerstrasse 100, D-14109 Berlin, Germany

J. Galin and B. Lott
GANIL (IN2P3-CNRS, DSM-CEA), BP 5027, F-14021 Caen-Cedex, France
(Received 7 January 1997)

Measurements of neutron multiplicity distributions of 1.94 to 5.0 GeV/*c* proton-, antiproton-, pion-, kaon-, and deuteron-induced spallation reactions on thin (few mm thick) and thick (35–40 cm thick) targets are presented. The 4π neutron detector employed for the first time to measure neutron multiplicity distributions from thick targets is described. Results for thin and thick targets are compared with intra- and internuclear cascade model calculations. [S0556-2813(97)02010-4]

PACS number(s): 25.40.Sc, 24.10.−i, 25.80.Hp, 29.25.Dz

I. INTRODUCTION

Spallation reactions have been mainly investigated so far by using energetic (GeV) protons. Very little is known about spallation reactions induced by mesons (pions, kaons), antiprotons, and light composite particles (such as deuterons). The major reason for this lack of experimental information stems from the weak intensity of these secondary particle beams (pions, kaons, antiprotons) which makes experiments difficult. However when choosing neutrons as the nuclear reaction probe, this problem can be overcome by using thicker targets than usually employed in nuclear physics experiments, g/cm^2 compared to mg/cm^2. Studying reactions induced in very thick (100 g/cm^2) targets is interesting in its own right; indeed, pions and kaons in addition to nucleons and composite particles are generated as the result of an initial proton interaction with a nucleus and they play an important role in subsequent reactions within a thick target. Spallation neutron sources (SNS's) for various applications, be it neutron scattering [1], transmutation [2] or energy amplifiers [3], exploit the thermal excitation induced by energetic (GeV) protons in heavy nuclei and the subsequent decay of these nuclei by evaporation of mainly neutrons with energies of a few MeV. Energetic (hundreds of MeV) particles (mainly nucleons but also pions, kaons, and composite particles such as deuterons) which are emitted during the initial excitation process can induce secondary reactions in thick targets producing additional neutrons. These processes are described by intra- (INC) and internuclear cascade models which are widely used to design SNS's. However, the reliability of these models is questionable in particular at energies above about 1 GeV where only few data exist. In order to test such models but also to identify possible deficiencies it is desirable not only to investigate the mean number of neutrons emitted per incident proton but more importantly the neutron multiplicity *distribution* which should be a sensitive benchmark to any such model. To this purpose we have launched a program to measure neutron multiplicity distributions of 2–5 GeV/*c* proton-, antiproton-, pion-, and deuteron-induced spallation reactions mainly on Pb targets of various geometries (0.2–36 cm long cylinders of 8–15 cm diameters) but also on Ag, Ho, Au, and depleted U targets.

So far only mean neutron multiplicities have been measured for *p*- and *d*-induced reactions and the variation of target geometries was very limited. A compilation of previous measurements was recently given elsewhere [4] where preliminary results of the present work have also been presented. No data exist at all for pion-induced reactions which are of importance to account for the yield of secondary reactions, with the pions being produced in a primary proton nucleus interaction. The first experiment which measured neutron multiplicity distributions for 0.475 and 2 GeV *p* bombarding thin targets was carried out at SATURNE/Saclay by Pienkowski *et al.* [5].

What further information can such multiplicity distributions provide compared to the mean values already measured?

(i) For thin targets (only one nuclear interaction in the target) the number of evaporative neutrons is a good measure of the distribution of the thermal excitation energy induced in the nucleus. In this sense the neutron multiplicity distribution is a sensitive test of the primary spallation process, i.e., the *intra*nuclear cascade part of the theoretical model. At high excitation energies above about 2–3 MeV/nucleon in heavy nuclei additional information [6] on light charged particles (evaporative protons and He) improves the excitation energy resolution by about a factor 2–3.

(ii) For thick targets (multiple reactions) the alteration of the neutron multiplicity distribution reflects the production of additional neutrons produced in secondary reactions and thus it is a sensitive test to both the *intra*- and *inter*nuclear cascade part of theoretical models.

In addition to the above-mentioned neutron measurements recently also light charged particles have been measured with $\pi, p, \overline{p}$, ^{3,4}He projetiles in the energy region of 1–14 GeV [6–11]. However, most of these studies measured energetic

*On leave of absence from University of Warsaw, Poland.
†Electronic address: HILSCHER@HMI.DE

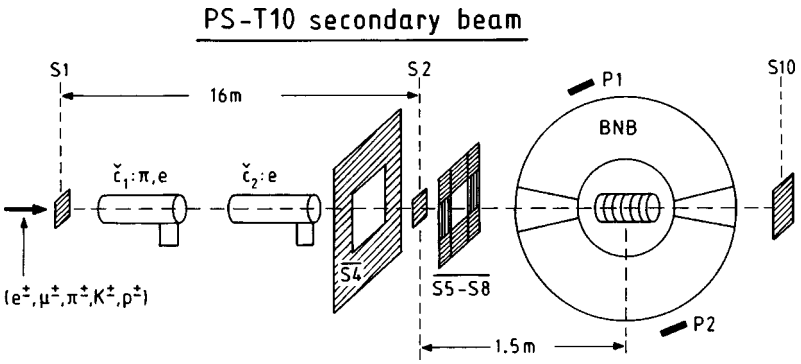

FIG. 1. Schematic setup at the secondary beam facility of the CERN-PS.

cascade and not evaporative light charged particles (p and He) which are needed to deduce thermal excitation energies.

In the following sections we describe the 4π neutron detector (Sec. II), the experimental setup at CERN (Sec. III), the experimental results and comparison with theoretical models (Sec. IV), and conclude with a discussion of the results (Sec. V).

II. 4π NEUTRON DETECTOR

The 4π neutron detector BNB (Berlin Neutron Ball) consists of a spherical vessel with outer and inner diameters of 140 and 40 cm, respectively. This 50 cm thick vessel is filled with 1500 l of scintillator liquid loaded with gadolinium (0.4% by weight). Neutrons produced in the target at the center of the reaction chamber are detected after being slowed down in the surrounding scintillator volume by elastic collisions with H atoms and captured by gadolinium nuclei.

The scintillator light registered with 24 fast photomultipliers distributed on the outer surface of the tank consists of two components separated in time.

(i) The *prompt light* observed within about 0.7 μs of the reaction is a measure of the summed energy of all charged particles (p, $\pi^{\pm}$, $K^{\pm}$, $e^{\pm}$ from γ rays) and γ rays emitted either from the target or resulting from the slowing down of neutrons via scattering or reaction on hydrogen and carbon. The prompt light in coincidence with the arrival time of an incident particle signals the occurrence of a nuclear reaction and thus can be exploited to measure the *total reaction cross section*. The light threshold was set to 10 MeVee (electron equivalent). Thus, the total reaction cross section measured in this way corresponds to an energy loss of at least 10 MeV.

(ii) The *delayed light* is due to the Gd-capture γ rays and is exploited to count the neutrons on an event-by-event basis for each reaction or in the case of a thick target for each incident particle. This number is the essential observable of this detector. Since the capture times for neutrons have a broad distribution with a mean value of about 15 μs the light flashes can be easily counted during a counting gate of about 45 μs.

The 4π neutron detector counts the number of neutrons which are produced by each reaction or each incident proton in the target with high efficiency of typically 85% for each evaporative (few MeV) neutron. The efficiency is continuously calibrated with a ^{252}Cf fission source. For higher neutron energies, BNB becomes progressively more transparent, the efficiency drops to 15% at 100 MeV.

The measured neutron multiplicity distribution has to be corrected for detection efficiency, dead time, correlated and uncorrelated background. The uncorrelated background as measured with no target has been subtracted. The correlated background has been measured on line in a second, 45 μs long gate, issued 400 μs after the first counting gate and has been corrected for by deconvolution. The loss of neutron counting due to the occurrence of two neutron captures within a fixed dead time of 35 ns has been corrected for by deconvolution as well. This dead time correction amounts to 6.7 and 13.1 % for neutron numbers of 30 and 50, respectively. Since the neutron energy is not measured an energy dependent efficiency correction is not possible, that is why only the measured distributions ($d\sigma/dN_{\mathrm{expt}}$) not corrected for efficiency are shown below. For comparison with theory we rather prefer to fold the calculated neutron multiplicity with the experimental detection efficiency at the calculated neutron energies. The *mean* neutron multiplicities $\langle M_n \rangle$ as well as the most probable neutron multiplicity $M_n^{\max}$ given below have been, however, corrected for an assumed average neutron detection efficiency of 85% as obtained from the Cf calibration. The same procedure was employed in all previous moderator measurements of mean values. It should be noted, however, that this is only a crude approximation assuming that the mean energy of all neutrons is only a few MeV.

The above described Gd-loaded detector type has been widely employed in recent years in order to measure the excitation energy generated in heavy-ion [12,13], light-ion [5,14], and antiproton- [6,15] induced reactions. It should be noted that due to the detection method this detector has essentially no lower energy detection threshold as it counts thermalized neutrons.

III. EXPERIMENTAL ARRANGEMENT

We describe here the experimental arrangement (Fig. 1) which we employed at the secondary beam line (T10) of the CERN-PS. Protons of 26 GeV were bombarding a 25 mm long and 4 mm diameter Cu production target with a duty cycle of about 2.5%, producing all kinds of particles. The charges (positive or negative) and momenta of these particles could be selected by a system of dipole magnets. The momentum analyzed particles were focused by quadrupoles onto the target inside BNB (about 40 m downstream the production target) to about 1–2 cm in diameter. The particle species, however, had to be identified by measuring the time of flight between two thin (2 mm) scintillator detectors $S1$

and $S2$ over a distance of 16 m. This TOF was sufficient to separate deuterons and protons from lighter particles (kaons, pions, muons, and positrons) up to 5 GeV/c. In order to separate also the lighter particles we had to exploit two Čerenkov counters $\check{C}_1$ and $\check{C}_2$ which triggered, respectively, on pions plus lighter particles and positrons only. Neutron multiplicity distributions could thus be registered simultaneously for reactions induced by p^+, π^+, K^+, e^+, and also d^+ on the one hand and by p^- and π^- on the other hand. Muons, however, could not be separated from pions. The large muon contamination of the incident beam made the determination of the reaction probability for pions uncertain but did not affect the neutron multiplicity distribution. In addition to $S1$ and $S2$ a system of veto counters $\overline{S4}$, $\overline{S5-S8}$ (inner opening 1–4 cm^2) were used to reject particles traveling off axis and/or hitting the neutron detector during the neutron counting gate. $S10$ was used to focus the beam through BNB.

The measurements at $E_p=1.22$ GeV were performed as part of experiment PS208 (devoted to the investigation of hot nuclei) at the low energy antiproton ring LEAR/CERN with protons (with almost 100% duty cycle) at the same energy as antiprotons used for another experiment [6]. The experimental setup was very similar except that we did not use $S2$ or any Cerenkov counters since we had here a pure and clean proton or antiproton beam extracted from LEAR.

Thin Ag, Ho, Au, and Pb targets were investigated as well as thick Pb and depleted U targets. The Pb targets had different diameters (8–15 cm) and thicknesses (0.2–36 cm). It was checked that the thick Pb targets made of standard lead brick shielding material contaminated by Sb did not differ from ultrapure Pb (provided to us by Andriamonje of the PS211 collaboration [16]) by more than 2.7% in the neutron production. The U targets, 8 cm in diameter and 40 cm long, were depleted (0.2% ^{235}U). The longest Pb and U targets that fit in the BNB ($l=40$ cm) correspond to about 2.1 and 3.5 reaction lengths or equivalently to a reaction probability of 88% or 97% in Pb or U, respectively. It should also be mentioned that the U target, because of its high intrinsic radioactivity, had to be shielded inside the BNB scattering chamber. The lateral shielding was made of 2 cm thick lead.

IV. RESULTS FOR 2–5 GEV/c P, $\overline{P}$, π, AND D+Pb AND U

In the following we present and discuss results for neutron multiplicity distributions $d\sigma/dN_{\rm exp}$, derived mean values, total reaction cross sections, and compare with intra- and internuclear cascade models.

A. Neutron multiplicity distributions

The distributions $d\sigma/dN_{\rm exp}$ of the number of measured neutrons ($N_{\rm exp}$) emitted in a single or in multiple reactions are shown in Fig. 2 for 1.22, 2.21, 3.17, and 4.15 GeV proton-induced reactions on thin ($l=0.2$–2 cm), intermediate ($l=5$, 10 cm), and thick ($l=35$ cm) Pb targets. For a 2 mm thick lead target the probability that reaction products from a primary reaction will induce a secondary reaction in the target is lower than 1% and thus the corresponding neutron

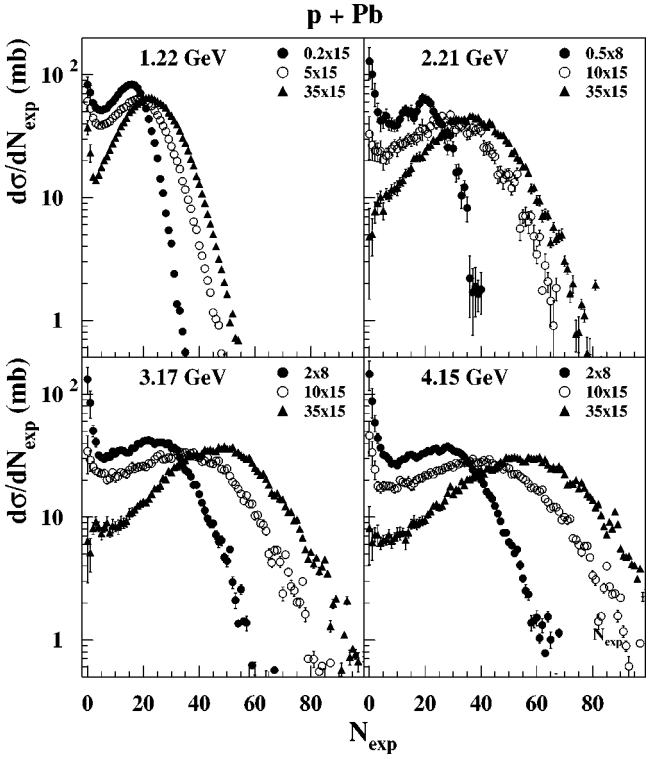

FIG. 2. Neutron multiplicity distributions for 1.22, 2.21, 3.17, and 4.15 GeV p+Pb for thin, intermediate, and thick targets. The measured number of neutrons $N_{\rm exp}$ have not been corrected for detection efficiency. The dimensions of the target are given in cm (thickness×diameter).

multiplicity distribution reflects the number of neutrons emitted in the primary spallation reaction.

In the case of thin targets the neutron multiplicity distribution can be characterized by a Gaussian distribution centered at high neutron numbers plus an almost exponential increase towards low neutron numbers. The rise of cross section at low neutron multiplicities is also observed for the measurements at 1.22 GeV which were carried out with the pure low background proton beam of LEAR/CERN without secondary beam particles. Thus it can be excluded that the low multiplicity component is due to the high background of the secondary beam which furthermore was carefully investigated and corrected for. The high and low multiplicity components can be associated with central and peripheral reactions, respectively, and have also been observed in charged particle multiplicity distributions in p- and π-induced reactions [8]. The central peak is observed to broaden and move to higher neutron multiplicity with increasing bombarding energy (see also Fig. 7). The probability of producing hotter nuclei in the upper tail of the distribution is thus increasing with bombarding energy as well. But since simultaneously the intensity in the peripheral peak at low neutron multiplicities is increasing, the first moment $\langle M_n\rangle$ of the distribution is found almost independent of the incident proton energy (Fig. 7). However, it must be pointed out here that the low neutron multiplicities for thin targets (below 2 cm) are uncertain for particle momenta above 1.94 GeV/c due to larger background for measurements carried out at the secondary beam facility of the CERN-PS. It is also visible in Fig. 2 that the 1.94 MeV/c data are of better quality. They have been ob-

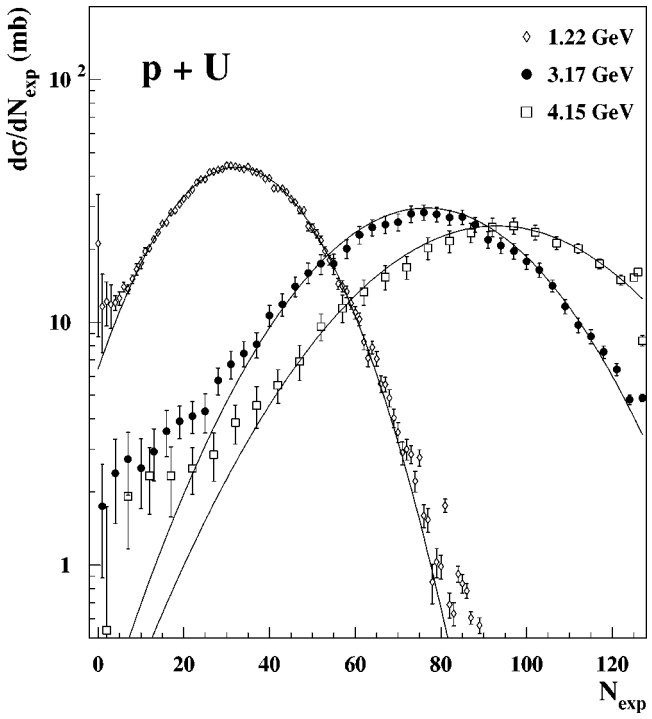

FIG. 3. Measured neutron multiplicity distributions for $p+$U. The depleted U target was 40 cm long with a diameter of 8 cm. At 3.17 and 4.15 GeV the U bar was surrounded by a 38 cm long lead cylinder with an inner and outer diameter of 8 and 15 cm, respectively. The solid lines are fits with a Gaussian distribution, the parameters are given in Table I.

tained with a high-quality beam at the LEAR ring delivering protons.

When the target thickness is increased the intensity of low neutron multiplicity events decreases due to secondary reactions while at the same time the centroid of the Gaussian distribution moves towards higher neutron numbers (see Fig. 2). The relative width ($\sigma/M_n^{\max}$) of the Gaussian part of the distributions remains almost constant between 0.4 and 0.5. It is interesting to note that the distributions of $\overline{p}$-induced reactions are narrower with $\sigma/M_n^{\max}=0.3$ to 0.4. This finding is probably caused by the peculiarity of the annihilation process which distributes already in the primary reaction the available energy on several (about 5) less energetic pions. For thick targets the measured neutron multiplicity distribution can be rather well described by a single Gaussian distribution. This is shown in Fig. 3 for a 40 cm long depleted U target by the solid lines.

The observed larger neutron multiplicity for U compared to Pb can be ascribed in the case of thin targets (see Table I) to a higher probability for energy absorption in the bigger target nucleus, to the lower neutron binding energies of U spallation products, and eventually to one or more extra neutrons from fission of the residual nucleus ($\overline{\nu}=1.92$ for spontaneous fission of ^{238}U). In a thick target of U fission can be induced by many secondary particles and become a dominating process (see Fig. 3). It multiplies the number of neutrons to the extent that the neutron yield in a 40 cm long U target is nearly doubled as compared to Pb: $\langle M_n^{\mathrm{U}}\rangle/\langle M_n^{\mathrm{Pb}}\rangle=1.5$ and 1.7 at $E_p=$ 1.22 and 4.15 GeV, respectively.

Finally the neutron multiplicity distributions for positive pion-induced reactions on a thick Pb target (35 cm long, 15 cm in diameter) were measured at the same incident momenta (2.0, 3.0, 4.0, and 5.0 GeV/c) as the proton data, corresponding to somewhat higher kinetic energies than the respective proton energies. The multiplicities are somewhat smaller than for protons if compared at the same incident energy (see Fig. 7).

TABLE I. Results for thin and thick Pb and depleted U targets: the mean neutron multiplicity $\langle M_n\rangle$, the number of neutrons per incident particle $\langle N_n\rangle/p$, the most probable neutron number $M_n^{\max}$, and the width σ, the latter two are obtained from a Gaussian fit. These values have been multiplied with 1/0.85 in order to account for an assumed mean detection efficiency of 85%. Errors are in the order of 1 to 5%. Negative momenta p correspond to antiprotons or negative pions, L and D indicate the target length and diameter, respectively.

		Protons						Pions π			
p GeV/c	T	L cm	D cm	$M_n^{\max}$	σ	$\langle M_n\rangle$	$\langle N_n\rangle/p$	$M_n^{\max}$	σ	$\langle M_n\rangle$	$\langle N_n\rangle/p$
1.94	Pb	0.2	15	18.0	7.4	14.5	0.16				
1.94	Pb	5.0	15	21.3	10.7	19.4	4.8				
1.94	Pb	35	15	26.0	11.5	25.4	20.5				
−1.94	Pb	35	15			52.4	35.3				
2.00	Pb	35	15	26.7	13.0	26.7	22.6	35.5	16.5	32.5	20.5
3.00	Pb	35	15	42.2	16.5	41.1	34.9	48.0	20.1	46.2	34.6
4.00	Pb	35	15	53.9	20.4	51.7	44.0	57.5	22.9	55.1	38.7
−4.00	Pb	35	15			72.2	65.6			60.5	47.0
5.00	Pb	35	15	63.8	24.5	60.8	51.0	66.0	27.8	63.3	50.1
−5.00	Pb	35	15			79.5	71.2			68.6	
1.94	U	0.3	5×5	23.3	8.8	19.9	0.53				
1.94	U	40	8	38.0	19.4	38.8	35.3				
4.00	U	40	8(15)	90.1	28.6	87.6	84.1	99.3	33.1	93.5	69.3
5.00	U	0.9	5×5	35.6	21.8	28.5	2.56	36.7	24.5	30.5	1.74
5.00	U	40	8(15)	112.2	30.5	106.0	101.0	115.3	36.1	107.5	72.4

B. Mean neutron multiplicities

In order to compare with previous measurements we discuss in the following also the first moment $\langle M_n \rangle$ of $d\sigma/dN_{\rm exp}$ as well as the most probable neutron number $M_n^{\rm max}$ as derived from a Gaussian fit to the multiplicity distribution $d\sigma/dN_{\rm exp}$ at the position of the maximum. From the measured reaction probability $P_{\rm reac}$ and $\langle M_n \rangle$ we deduce the mean number of neutrons per incident proton $\langle N_n \rangle / p = \langle M_n \rangle \times P_{\rm reac}$ which is of practical interest for the design of spallation neutron sources. Some of the above-defined observables deduced from the measured neutron multiplicity distributions are given in Table I for protons, antiprotons, positive and negative pions.

For protons we observe with increasing target thickness an increase of both the mean neutron multiplicity $\langle M_n \rangle$ as well as the most probable neutron multiplicity $M_n^{\rm max}$ with the relation $\langle M_n \rangle \leqslant M_n^{\rm max}$ (see Fig. 4). For the thickest targets of 35 cm Pb $\langle M_n \rangle$ has almost attained the value of $M_n^{\rm max}$ (Table I) simply due to the fact that the intensity of low neutron multiplicity events has become very small due to secondary reactions. For 35 cm Pb as well as 40 cm U the intensity of the measured distribution which cannot be described by a Gaussian is smaller than 5% while for thin targets it amounts to 20–30 %. For target thicknesses larger than 35 for Pb or 40 cm for U any further increase of the neutron yield per incident proton $\langle N_n \rangle / p$ is essentially due only to further increase of the reaction probability. The observed steep increase of the number of neutrons per incident proton $\langle N_n \rangle / p$ (Fig. 4, middle panel) for target thicknesses up to about 10 cm, instead, is due to the combined increase of the reaction probability $P_{\rm reac}$ and the mean neutron multiplicity $\langle M_n \rangle$ with target thickness. Contrary to other methods these two quantities are measured independently in the present experiment and not as a product.

For Pb targets we have also investigated the combined effect of the target diameter and thickness on neutron production (Fig. 4). With increasing proton energies from 1.22 to 4.15 GeV we observe an increase of the ratio of the mean neutron multiplicities $\langle M_n^{15} \rangle / \langle M_n^{8} \rangle$ for a 35 cm long and 15 to 8 cm in diameter target from 1.17 to 1.28. This indicates that at 4.15 GeV proton energy targets with a larger diameter would further increase the neutron production.

In the top panel of Fig. 4 we show also the measured survival probability of the incident protons without interaction which follows the expected exponential absorption law $(1 - P_{\rm reac}) = \exp(-L/L_{\rm reac})$ with a reaction length $L_{\rm reac} = 18.4$ cm, corresponding to a cross section of 1.65 b. For thinner Pb targets (2 cm) we deduce, however, a larger reaction cross section of 1.73, 1.83, 1.89, and 1.87 b for proton momenta of 1.94, 3, 4, and 5 GeV/c, respectively. The latter values agree quite well with the expected [17] inelastic cross section of about 1.9 b for proton induced reactions on lead in this energy region.

When comparing the present data with those of Vassilkov *et al.* [18] for a 60 cm long and 20 cm in diameter Pb target, the former data are increasingly smaller for larger incident proton energy. We ascribe this neutron production difference to the smaller size of the target and in particular the smaller diameter used in the present experiment. Indeed we know from our measurements that the neutron multiplicity is still

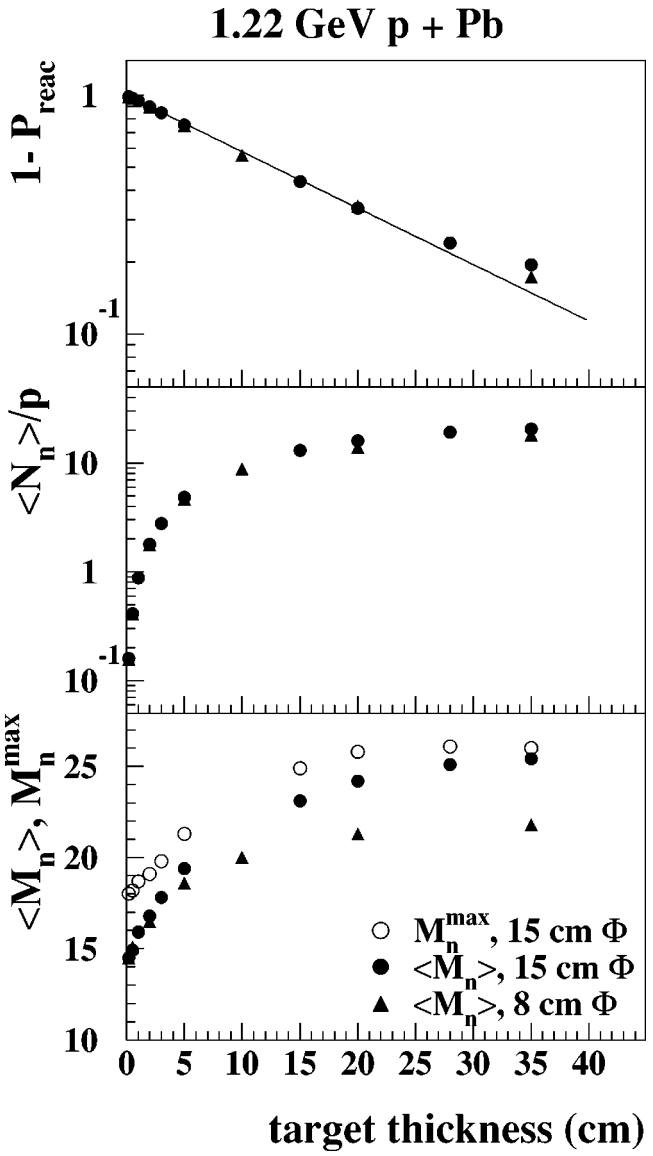

FIG. 4. Survival probability $1 - P_{\rm reac}$, mean number of neutrons per incident proton $\langle N_n \rangle / p$, and mean neutron multiplicity $\langle M_n \rangle$ and most probable neutron multiplicity $M_n^{\rm max}$ (from Gauss fit) as a function of target thickness. $\langle N_n \rangle / p$, $\langle M_n \rangle$, and $M_n^{\rm max}$ have been corrected for a mean efficiency of 0.85.

increasing with diameter at 4.15 GeV whereas at lower energies the effect is much smaller. The corresponding results for the thick depleted U targets are found to agree very well with the data of the pioneering work of Fraser *et al.* [19] in the overlapping energy region close to 1.2 GeV.

In summary the deduced mean values from the measured neutron multiplicity distributions (corrected for a mean efficiency) agree well with previous measured mean values when taking into account the somewhat different target geometries. However, it should be stressed again that the present data enable a much more sensitive test for high energy transport codes like the HERMES code [20]. Such comparisons will be presented and discussed below.

C. Comparison with inter- and intranuclear cascade calculations

In Fig. 5 we show measured neutron multiplicity distributions for thin targets of Ag, Ho, Au, and Pb at $E_p = 1.22$

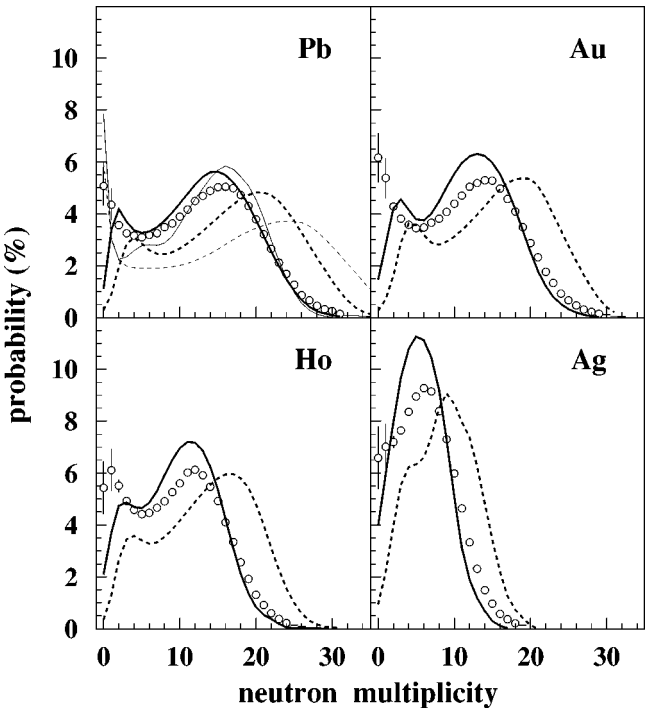

FIG. 5. Neutron multiplicity distributions for 1.22 GeV proton-induced reactions on thin targets of Ag (2.1), Ho (5.3), Au (1.9), and Pb (2.3 g/cm^2). The thick dashed lines are the results of INC [21] + GEMINI [22] calculations which were folded as a function of neutron energy with the detection efficiency [4] as shown by the thick solid lines. The respective results obtained with the HERMES code for a Pb target are shown by the thin solid and dashed lines.

GeV. We note the almost linear increase of the most probable neutron multiplicity ($M_n^{\max}$) with atomic mass of the target nucleus reflecting the increase of energy absorption with target mass as well as the increasing predominance of neutron evaporation over charged particle emission due to the increase of the Coulomb barrier hindering charged particle emission.

The data are compared with the result of a two-step model consisting of an intranuclear cascade (INC) calculation using the code of Cugnon [21] for the initial stage of the reaction until thermal equilibrium is approached after about 30 fm/c (see also Pienkowski *et al.* [5]). At this stage the deexcitation of the nucleus is followed by the evaporation code GEMINI [22], with the level density parameter taken as $A/10$ MeV^{-1}. The thick dashed line in Fig. 5 represents the output of the two-step calculation whereas the thick solid line also makes allowance for the detector response. This correction, being dependent on the neutron energy, takes into account the energies of the directly emitted neutrons of the INC code as well as those of the evaporated neutrons of the subsequent GEMINI code. The mean values $\langle M_n \rangle = 12.5$ (16.5), 11.2 (15.2), 9.62 (13.4), 5.68 (8.7) deduced from the calculated distributions folded with the detection efficiency (in parentheses without this correction) for Pb, Au, Ho, and Ag, respectively, agree quite well with the respective first moments 12.3, 11.0, 9.3, 6.2 of the *measured* distributions, not corrected for efficiency. However, by comparing the calculated and measured distributions we observe for low ($\leqslant 2$) neutron multiplicities a considerable discrepancy between calculation and experiment whereas at higher neutron numbers the overall agreement is much better. The deviation at low neutron multiplicity results from the assumption of a sharp cutoff nuclear density distribution used in the model, leading to an unrealistic description of peripheral reactions. This example stresses the methodical advantage of neutron multiplicity distributions in deducing the origin of possible deficiencies of theoretical models.

It would be interesting to compare the present results also with a quantum molecular dynamics code for the initial stage of the reaction followed by a statistical decay model which was quite successful in describing neutron energy spectra for thin targets [23] as well as charged particle production yields [24].

For Pb we also show by the thin solid and dashed lines in Fig. 5 the results obtained with the Bertini-type [25] INC code incorporated in the high energy transport code HERMES of Cloth *et al.* [20] plus subsequent evaporation. In this INC code the nuclear density of a nucleus is somewhat more realistically modeled by subdividing the radial dependence into three zones. The level density parameter for evaporation was taken to be $A/14$ MeV^{-1}.

For a thin Pb target we observe with this code a better agreement with the experimental neutron multiplicity distribution in particular for low neutron numbers though the contribution for zero neutrons is larger than measured. Combining these results of the INC part of the HERMES code with the internuclear cascade part of this code we compare the results for a thick (35 cm long) Pb target in Fig. 6 with the measured neutron multiplicity distribution for proton energies of 1.22, 2.21, 3.17, and 4.15 GeV. The dashed (solid) line shown in Fig. 6 corresponds to the result of the HERMES calculation without (with) correction for the neutron energy dependent detection efficiency of the employed 4π neutron detector. The solid curves have to be compared with the measured distributions shown by the open circles. The agreement between calculation and experiment is astoundingly good and considerably better than the results for a thin target (see Fig. 5). This seems to indicate that the combination of inter- and intranuclear cascade codes corrects deficiencies in the INC part, less energy transfer in the primary interaction leads to more kinetic energy and thus to more excitation in the secondary reaction and vice versa. With increasing incident proton energy, however, we observe a small but increasing deviation of the calculated neutron multiplicity distribution to larger neutron numbers. This can also be seen from the numbers given in Table II where the mean or most probable neutron number deviates by about 10% at 5 GeV/c.

In summary, we have shown in this section the advantage of measuring the whole neutron multiplicity distributions instead of single average values. This brings much more constraint to the INC model. Also the measurements in both thin and thick targets appear quite complementary since, in thick targets, compensation effects between the first reaction and secondary reactions can mask deficiencies in reproducing the primary reaction by the INC model. The thick target measurement brings an additional, although indirect, test of the thin target measurement insofar as it allows one to follow the fate of the products of the primary interaction in generating extra neutrons.

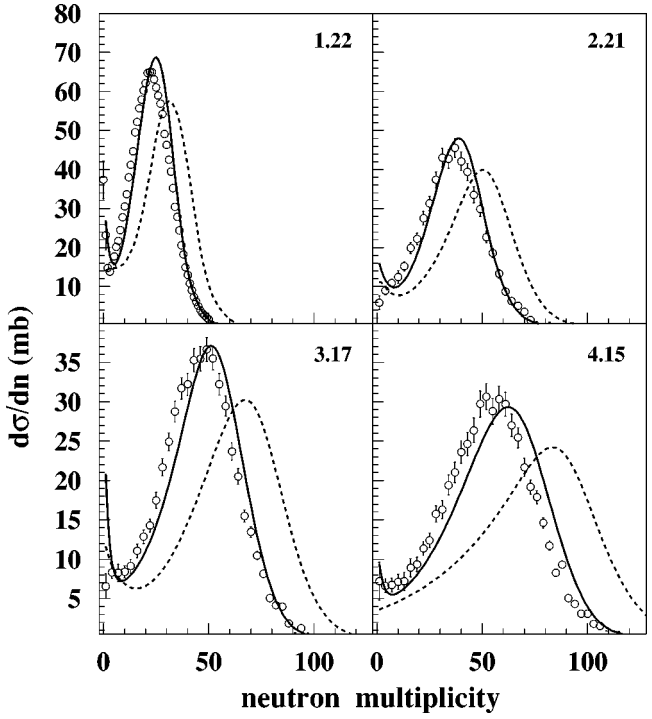

FIG. 6. Neutron multiplicity distributions for 1.22, 2.21, 3.17, and 4.15 GeV proton-induced reactions on a 35 cm long and 15 cm diameter Pb target. The measurement is shown by the open circles, the solid (dashed) line correspond to the HERMES calculation [20] corrected (not corrected) for the detector efficiency [4].

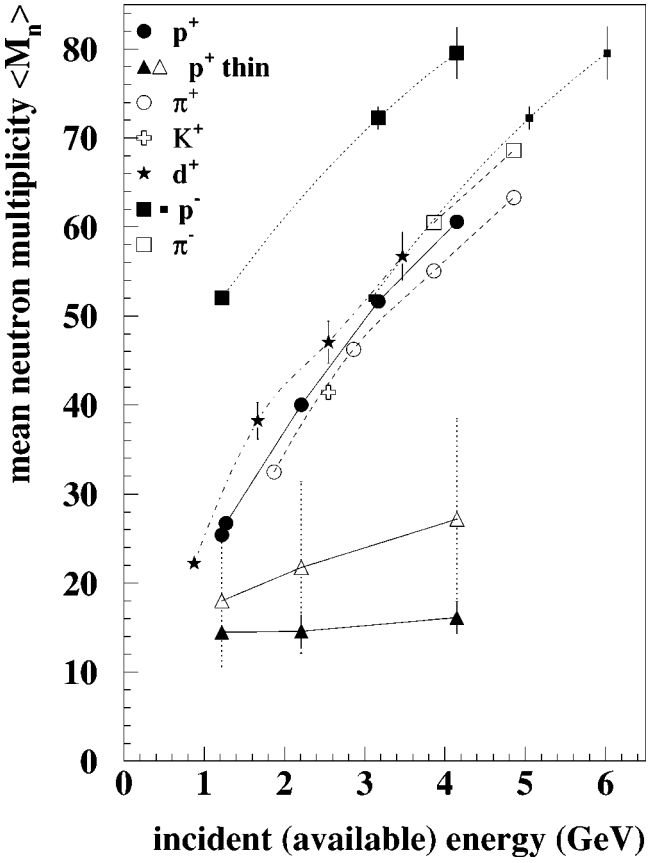

FIG. 7. Mean neutron multiplicity $\langle M_n \rangle$ for incident protons p^+, pions $\pi^{\pm}$, deuterons d^+, and antiprotons p^- as a function of incident kinetic energy on a 35 cm long lead target with a diameter of 15 cm. The mean neutron multiplicity has been corrected for a mean efficiency of $\epsilon = 0.85$. The curves connect the data points. For $\overline{p}$ the smaller filled squares are plotted also at the *available* incident energy, see text. The filled and open triangles display $\langle M_n \rangle$ and $M_n^{\max}$, respectively, for thin (2 to 5 mm) Pb targets. The dashed vertical bars at the open triangles indicate the widths σ of the Gaussian fit.

D. Dependence of mean values on incident energy

Besides the dependence on target material and geometry it is also of particular interest to know how the mean neutron multiplicity depends on the incident energy and how protons compare with other light particles like deuterons, pions, kaons, and antiprotons. The data are shown in Fig. 7 where the mean neutron multiplicities induced by 2, 3, 4, and 5 GeV/c protons p^+, antiprotons p^-, deuterons d^+, kaons K^+, and pions $\pi^{\pm}$ are given as a function of energy. For a 35 cm thick Pb target we observe that the mean neutron multiplicities for protons are slightly larger or smaller than for positive pions or deuterons, respectively. Since the reaction cross section is also somewhat larger for deuterons than for protons this finding implies for the neutron yield per incident deuteron $\langle N_n \rangle / p = P_{\text{reac}} \times \langle M_n \rangle$ even larger values which qualitatively agree with the findings of Vassilkov *et al.* [18]. However, the uncertainty for deuterons in the present experiment is considerably larger since the secondary beam of the CERN-PS contains much less deuterons than protons (2 and $8) \times 10^{-3}$ at 5 and 3 GeV/c, respectively. In this respect it is also interesting to note that the mean neutron multiplicity for

TABLE II. Comparison of experimental and calculated (HERMES) [20] results for a 35 cm long and 15 cm diameter Pb target. The calculated neutron leakage out of the target has been folded with the neutron energy dependent BNB efficiency. The primary neutron leakage is given in parenthesis. $\langle M_n \rangle$ and rms are the first moment and the corresponding root mean square deviation, $M_n^{\max}$ and σ are obtained from a Gaussian fit to the measured or calculated distributions.

	Experiment					HERMES			
p GeV/c	$\langle M_n \rangle$	rms	$M_n^{\max}$	σ	P_{reac}	$\langle M_n \rangle$	rms	$M_n^{\max}$	σ
1.94	21.6	10.4	22.1	9.8	0.81	23.1(29.0)	10.0(12.2)	24.1(30.8)	9.1(10.7)
3.00	35.0	15.0	35.9	14.0	0.85	35.6(45.2)	14.8(18.3)	38.0(49.2)	12.7(14.8)
4.00	44.0	18.7	45.8	17.3	0.85	45.8(58.7)	19.4(24.3)	50.1(64.6)	15.8(19.7)
5.00	51.7	22.5	54.2	20.8	0.84	56.2(72.4)	23.1(29.1)	60.3(78.3)	21.2(25.8)

negative pions π^- is about 5 neutrons larger than for positive pions which would just correspond to the additional neutrons produced by a pion capture in a Pb nucleus.

As already seen on thin targets [6] the mean neutron multiplicity of $\bar{p}$+Pb on thick targets is considerably larger than for p+Pb if compared at the same incident kinetic energy. The available incident energy for antiprotons is, however, given by the kinetic energy plus the $N\bar{N}$ annihilation energy $2\times m_N c^2 = 1.88$ GeV (m_N nucleon mass). Performing the comparison at the same incident available energy $E_{\bar{p}} + 2\times m_N c^2$ we find that the mean neutron multiplicities of p- and $\bar{p}$-induced reactions are very similar for thick targets.

In summary the mean neutron multiplicity of π-, K-, p-, $\bar{p}$-, and d-induced reactions on thick targets are relatively similar if compared at the same incident available energy increasing from about 22 neutrons at 1 GeV to 80 neutrons at 6 GeV. The mean neutron multiplicities for antiproton-, negative-pion-, and deuteron-induced reactions are somewhat larger (5%) than for protons while positive-pion- and kaon-induced reactions result in somewhat smaller values.

V. CONCLUSIONS

We have measured for the first time neutron multiplicity *distributions* for hadrons in the GeV energy range, in particular proton-induced spallation reactions in thin and thick targets of several materials. The motivation of this work was mainly to provide sensitive data for testing existing models describing the intra- as well as internuclear cascades. These models are essential ingredients for the design and construction of accelerator driven neutron sources and thus it is important to detect and isolate possible deficiencies in the models. It was not the purpose of this work to compare our data with a large variety of different codes presently being used by various groups. We have, however, shown in one case how one can exploit the calculated and measured distributions to deduce the physical origin of a model deficiency although the measured mean values agreed quite well.

We have parametrized the measured neutron multiplicity distributions for various target thicknesses of Pb and depleted U with Gaussians and given the parameters in order to provide an easily accessible experimental data base as a testing ground for various intra- and internuclear cascade models.

For thick targets the calculated distributions, once corrected for neutron detection efficiency, agree rather well with the measured distributions though for thin targets, that is for the primary spallation reaction, the agreement is not quite as good indicating a compensation effect between intra- and internuclear cascade calculations. For proton-induced spallation reactions on a 35 cm long lead target the calculated neutron multiplicities exceed the measured ones by 10% at most.

ACKNOWLEDGMENTS

We would like to thank X. Ledoux, E. Liénard, B. Quednau, W.-U. Schröder, and J. Tõke for taking part in some of the measurements, R.-D. Neef and D. Filges for performing the HERMES calculations and for discussions, L. Durieu and E. Widmann for continuous support at CERN. This work was supported by the project for a design study of a European Spallation Source.

[1] J. M. Carpenter, Nucl. Instrum. Methods **145**, 91 (1977).

[2] C. D. Bowman, E. D. Arthur, P. W. Lisowski, G. P. Lawrence, R. J. Jensen, J. L. Anderson, B. Blind, M. Cappiello, J. W. Davidson, T. R. England, L. N. Engel, R. C. Haight, H. G. Hughes III, J. R. Ireland, R. A. Krakowski, R. J. LaBauve, B. C. Letellier, R. T. Perry, G. J. Russell, K. P. Staudhammer, G. Versamis, and W. B. Wilson, Nucl. Instrum. Methods Phys. Res. A **320**, 336 (1992).

[3] F. Carminati, C. Gelès, R. Klapisch, H. Ravn, J. P. Revol, Ch. Roche, J.A. Rubio, and C. Rubbia, CERN Report CERN/AT/93-47 (ET), 1993, S. Andriamonje *et al.*, Phys. Lett. B **348**, 697 (1995).

[4] D. Hilscher, F. Goldenbaum, U. Jahnke, L. Pienkowski, J. Galin, B. Lott, and B. Quednau, in *Proceedings of the International Workshop on Nuclear Methods for Transmutation of Nuclear Waste*, Dubna, edited by M. Kh. Khankhasayev, H. S. Plendl, and Z. B. Kurmanov (World Scientific, Singapore, 1997), p. 176.

[5] L. Pienkowski, H. G. Bohlen, J. Cugnon, H. Fuchs, J. Galin, B. Gatty, B. Gebauer, D. Guerreau, D. Hilscher D. Jacquet, U. Jahnke, M. Josset, X. Ledoux, S. Leray, B. Lott, M. Morjean, A. Péghaire, G. Röschert, H. Rossner, R. H. Siemssen, and C. Stéphan, Phys. Lett. B **336**, 147 (1994).

[6] F. Goldenbaum, W. Bohne, J. Eades, T. von Egidy, P. Figuera, H. Fuchs, J. Galin, Ye. S. Golubeva, K. Gulda, D. Hilscher, A. S. Iljinov, U. Jahnke, J. Jastrzebski, W. Kurcewicz, B. Lott, M. Morjean, G. Pausch, A. Péghaire, L. Pienkowski, D. Polster, S. Proschitzki, B. Quednau, H. Rossner, S. Schmid, S. Schmid, W. Schmid, and P. Ziem, Phys. Rev. Lett. **77**, 1230 (1996).

[7] S. Ahmad, B. E. Bonner, J. A. Buchanan, C. S. Chan, J. M. Clement, S. E. Eiseman, A. Empl, A. Etkin, K. J. Foley, R. W. Hackenburg, T. J. Hallman, M. A. Kramer, J. Krug, S. J. Lindenbaum, R. S. Longacre, W. A. Love, L. Madansky, W. Morris, G. S. Mutchler, D. C. Peaslee, E. D. Platner, A. C. Saulys, and S. Toshkov, Nucl. Phys. **A558**, 393c (1993).

[8] K. Nakai, T.-A. Shibata, H. Enyo, S. Sasaki, M. Sekimoto, I. Arai, K. Nakayama, K. Ichimaru, H. Nakamura-Yokota, and R. Chiba, Phys. Lett. **121B**, 373 (1983).

[9] K. Kwiatkowski, K. B. Morley, E. Renshaw Foxford, D. S. Bracken, V. E. Viola, N. R. Yoder, R. Legrain, E. C. Pollacco, C. Volant, W. A. Friedman, R. G. Korteling, J. Brzychczyk, and H. Breuer, Phys. Rev. Lett. **74**, 3756 (1995).

[10] W.-c. Hsi, K. Kwiatkowski, G. Wang, D. S. Bracken, H. Breuer, Y. Y. Chu, E. Cornell, F. Gimeno-Nogues, D. S. Ginger, S. Gushue, M. J. Huang, R. G. Korteling, W. G. Lynch, K. B. Morley, E. Ramakrishnan, L. P. Remsberg, D. Rowland, M. B. Tsang, V. E. Viola, S. J. Yennello, N. R. Yoder, and H. Xi, *Proceedings of XIII Winter Workshop on Nuclear Dynamics*,

Marathon, 1997, Report INC-40007-117.
[11] V. Lips, R. Barth, H. Oeschler, S. P. Avdeyev, V. A. Karnaukov, W. D. Kuznetsov, L. A. Petrov, O. V. Bochkarev, L. V. Chulkov, E. A. Kuzmin, W. Karcz, W. Neubert, E. Norbeck, and D. H. E. Gross, Phys. Lett. B **338**, 141 (1994).
[12] J. Galin and U. Jahnke, J. Phys. G **20**, 1105 (1994).
[13] J. Tõke, B. Lott, S. P. Baldwin, B. M. Quednau, W. U. Schröder, L. G. Sobotka, J. Barreto, R. J. Charity, D. G. Sarantites, and D. W. Stracener, Phys. Rev. Lett. **75**, 2920 (1995).
[14] J. Galin, D. Hilscher, H.G. Bohlen, J. Cugnon, H. Fuchs, B. Gatty, B. Gebauer, D. Guerreau, D. Jacquet, U. Jahnke, M. Josset, X. Ledoux, S. Leray, B. Lott, M. Morjean, A. Péghaire, L. Pienkowski, G. Röschert, H. Rossner, R. H. Siemssen, and C. Stéphan, *Proceedings of 8th Journées SATURNE on Accelerators Applied to the Nuclear Waste Problem*, Saclay, 1994, LNS/Ph/94-12, p. 79.
[15] U. Jahnke, W. Bohne, J. Eades, T. von Egidy, P. Figuera, H. Fuchs, J. Galin, F. Goldenbaum, K. Gulda, Ye. S. Golubeva, F. J. Hartmann, D. Hilscher, A. S. Iljinov, J. Jastrzebski, W. Kurcewicz, B. Lott, M. Morjean, G. Pausch, A. Péghaire, L. Pienkowski, D. Polster, S. Proschitzki, B. Quednau, H. Rossner, S. Schmid, S. Schmid, and W. Schmid, Yad. Fiz. **59**, 1625 (1996) [Phys. At. Nucl. **59**, 1567 (1996)].
[16] C. Rubbia *et al.*, PS211 Collaboration, CERN Report SPSLC/95-17/P291.
[17] A. Fasso, K. Goebel, M. Höfert, J. Ranft, and G. Stevenson, in Landolt Börnstein, New Series, Group 1, Vol. 11, edited by H. Schopper (Springer-Verlag, Berlin, 1990), and references therein, p. 71.
[18] R. G. Vassilkov, V. I. Yurevich, Proceedings ICANS-XI, Tsukuba, 1990, p. 340.
[19] J. S. Fraser, R. E. Green, J. W. Hilborn, and J. C. D. Milton, Phys. Can. **21**, 17 (1966); T. W. Armstrong, P. Cloth, D. Filges, and R. D. Neef, Nucl. Instrum. Methods Phys. Res. A **222**, 540 (1984).
[20] P. Cloth, D. Filges, R.-D. Neef, G. Sterzenbach, Ch. Reul, T. W. Armstrong, B. L. Colborn, B. Anders, and H. Brückmann, Julich Report Jül-2203, 1988.
[21] J. Cugnon, Nucl. Phys. **A462**, 751 (1987).
[22] R. J. Charity, M. A. McMahan, G. J. Wozniak, R. J. McDonald, L. G. Moretto, D. G. Sarantites, L. G. Sobotka, G. Guarino, A. Pantaleo, L. Fiore, A. Gobbi, and K. D. Hildebrand, Nucl. Phys. **A483**, 371 (1988).
[23] K. Niita, S. Chiba, T. Maruyama, T. Maruyama, H. Takada, T. Fukahori, Y. Nakahara, and A. Iwamoto, Phys. Rev. C **52**, 2620 (1995).
[24] S. Chiba, O. Iwamoto, T. Fukahori, K. Niita, T. Maruyama, T. Maruyama, and A. Iwamoto, Phys. Rev. C **54**, 285 (1996).
[25] H. W. Bertini, Phys. Rev. C **6**, 631 (1973).